Patient-specific estimation of detailed cochlear shape from clinical CT images

Kjer, H Martin; Fagertun, Jens; Wimmer, Wilhelm; Gerber, Nicolas; Vera, Sergio; Barazzetti, Livia; Mangado, Nerea; Ceresa, Mario; Piella, Gemma; Stark, Thomas

Total number of authors:
16

Published in:
International Journal of Computer Assisted Radiology and Surgery

Link to article, DOI:
10.1007/s11548-017-1701-7

Publication date:
2018

Document Version
Peer reviewed version

International Journal of Computer Assisted Radiology and Surgery
https://doi.org/10.1007/s11548-017-1701-7

ORIGINAL ARTICLE

Patient-specific estimation of detailed cochlear shape from clinical CT images

H. Martin Kjer[1] · Jens Fagertun[1] · Wilhelm Wimmer[2] · Nicolas Gerber[2] · Sergio Vera[3] · Livia Barazzetti[4] · Nerea Mangado[5] · Mario Ceresa[5] · Gemma Piella[5] · Thomas Stark[6] · Martin Stauber[7] · Mauricio Reyes[4] · Stefan Weber[2] · Marco Caversaccio[8] · Miguel Ángel González Ballester[5,9] · Rasmus R. Paulsen[1]

Received: 24 June 2017 / Accepted: 28 December 2017

Abstract

Purpose A personalized estimation of the cochlear shape can be used to create computational anatomical models to aid cochlear implant (CI) surgery and CI audio processor programming ultimately resulting in improved hearing restoration. The purpose of this work is to develop and test a method for estimation of the detailed patient-specific cochlear shape from CT images.

Methods From a collection of temporal bone μCT images, we build a cochlear statistical deformation model (SDM), which is a description of how a human cochlea deforms to represent the observed anatomical variability. The model is used for regularization of a non-rigid image registration procedure between a patient CT scan and a μCT image, allowing us to estimate the detailed patient-specific cochlear shape.

Results We test the accuracy and precision of the predicted cochlear shape using both μCT and CT images. The evaluation is based on classic generic metrics, where we achieve competitive accuracy with the state-of-the-art methods for the task. Additionally, we expand the evaluation with a few anatomically specific scores.

Conclusions The paper presents the process of building and using the SDM of the cochlea. Compared to current best practice, we demonstrate competitive performance and some useful properties of our method.

Keywords Statistical shape model · Segmentation · Cochlear implant · Intracochlear anatomy · CT · Micro-CT

Introduction

Cochlear implants (CI) have become an established and successful way of treating severe hearing impairment and deafness. In the top performing cases, recipients achieve near-normal speech perception, but a large variability in the auditory restoration outcomes remains a challenge to be dealt with [28]. One of several solutions is to achieve a better understanding of the individual cochlear shape, as this allows customizing and optimizing of the surgical planning and subsequent CI programming according to the specific recipient [18]. Preoperative computed tomography (CT) scans are routinely performed during the assessment of CI candidacy, in order to roughly estimate the size of the cochlea and to plan the surgical procedure. However, intracochlear structures, such as the basilar membrane, cannot be sufficiently visualized, and it remains very challenging to extract information of individual cochlear anatomy from clinical CT images.

✉ H. Martin Kjer
hmkj@dtu.dk

1 Department of Applied Mathematics and Computer Science, Technical University of Denmark, Lyngby, Denmark

2 ARTORG Center for Biomedical Engineering Research, University of Bern, Bern, Switzerland

3 Alma IT Systems, Barcelona, Spain

4 Institute for Surgical Technology and Biomechanics, University of Bern, Bern, Switzerland

5 Department of Information and Communication Technologies, University Pompeu Fabra, Barcelona, Spain

6 Department of Otorhinolaryngology, Technical University Munich, Munich, Germany

7 Scanco Medical AG, Brüttisellen, Switzerland

8 Department of ENT, Head and Neck Surgery, Inselspital, University of Bern, Bern, Switzerland

9 Catalan Institution for Research and Advanced Studies (ICREA), Barcelona, Spain

Published online: 06 January 2018

Image processing strategies have been developed to improve the visual quality of the CT data [27], and there are also different approaches for predicting the true patient cochlear anatomy based on the sparse information of the CT scan. One way is to estimate the "global" morphometrics of the cochlea by fitting various spiral models to the data [7,8,10]. These studies are characterized by measurements of a few observable parameters, such as the cochlear height and the basal turn diameter, from which additional morphometrics are inferred using idealized mathematical spiral formulations. Another reported strategy [2] uses a model-to-image-based optimization procedure. The approach is to estimate nine shape parameters of a 3D spiral shell model, which is done by fitting the surface to image edge features (gradient magnitude and orientation with respect to the surface normal) of the CT data. None of these methods are able to account for the true regional variability and can only represent generic shapes. For instance, with such methods all cross sections of the cochlea are perfectly circular, contrary to what can be observed from high-resolution anatomical studies [1]. Naturally, this puts a limit on the accuracy of predicting the correct patient-specific anatomy.

These approaches are perfectly logical and sensible under the assumption that the CT images are all one has to work with. The anatomical information available in this data is very limited. Intracochlear structures like the *basilar membrane* and *spiral lamina ossea* are completely invisible, and even the complete gross geometry of the cochlear spiral can be difficult to observe and describe fully. A strategy to advance further therefore requires learning about the cochlear anatomy beforehand. A learning-based strategy involves training a model of the anatomy and its population variability from high-resolution μCT datasets. This model can be based on a much larger number of parameters to describe not only the overall shape but also some intracochlear anatomy. The accurate model is then adapted to the sparse anatomical information provided by the CT data using an optimization method.

One of the most successful learning-based approach to date [17] uses an active shape model (ASM) [5] of the cochlea built from a small selection of ex vivo μCT scans. The learned statistical model provides a shape prior, which can regularize a registration procedure between a patient CT scan and a CT-atlas enhanced with a model of the detailed cochlear anatomy.

This study follows a strategy along the same principles. We start from an accurate high-resolution computational model of the cochlea extracted from μCT data [3]. Non-rigidly adapting this model to a patient CT scan will provide a patient-specific estimation of the anatomy. Using a selection of training μCT datasets, we extract a statistical deformation model (SDM) [22], describing statistically in which ways a μCT scan can deform to match another cochlear shape. During an image registration process, the SDM acts as a regularizing shape prior. This allows us to adapt the computational model to a clinical CT scan, ensuring anatomically plausible outputs. Compared to the method of [17], we present an alternative to using statistical shape modeling (SSM) methodology to tackle the same problem. The SSM approach uses a mesh-to-volume registration, where a set of surface points are fitted to the gradients of the target image. The proposed approach uses instead a volume-to-volume registration. The advancement lies partly in the methodology and partly in the underlying data, both contributing to an estimation of more anatomically accurate models with an arguably better potential for computational applications. The paper presents and evaluates the overall framework for building a SDM of the cochlea from high-resolution μCT data and the application of the subsequent SDM-regularized fitting procedure to preoperative CT data.

Materials and methods

Data and segmentation

Anatomical reference model The method builds up from a reference dataset where the cochlear spiral and certain intracochlear structures can be seen and segmented. We use the μCT scan from [3]. In short, it is a human temporal bone, which is cut to contain the cochlea and most of the vestibule and then preserved by freezing. It was scanned using a commercial μCT (μCT 50, Scanco Medical AG, Brüttisellen, Switzerland) and reconstructed in isotropic 5.9 µm voxels. The preparation and high resolution allowed for a manual segmentation of the cochlear spiral and the cochlear partition (approximation to the basilar membrane) (see Fig. 1 top left). A 3D surface model with these structures was generated from the segmentation using Marching Cubes [14] followed by a surface reconstruction [19] to obtain a well-formed triangulated mesh (see Fig. 1 right). The model forms the basis for a cochlear computational model suited for simulating for instance CI surgery and the effect of CI placement.

Training data Additional scans are needed for learning the anatomical variability. The μCT training data for building a statistical deformation model (SDM) (see "SDM-regularized registration" section) consists of 18 dried temporal bone specimens without major deviations from the normal cochlear anatomy. The samples were scanned with a commercial μCT (μCT 100, Scanco Medical AG, Brüttisellen, Switzerland) and processed to obtain isotropic voxels of 24.5 µm. Due to being dried bones, no soft tissues are present in the images. The cochlear lumen was segmented as a single object (see Fig. 1), using the semiautomatic tools available in ITK-SNAP [30] for doing the bulk of the work. However, manual corrections were needed to remove obvious errors,

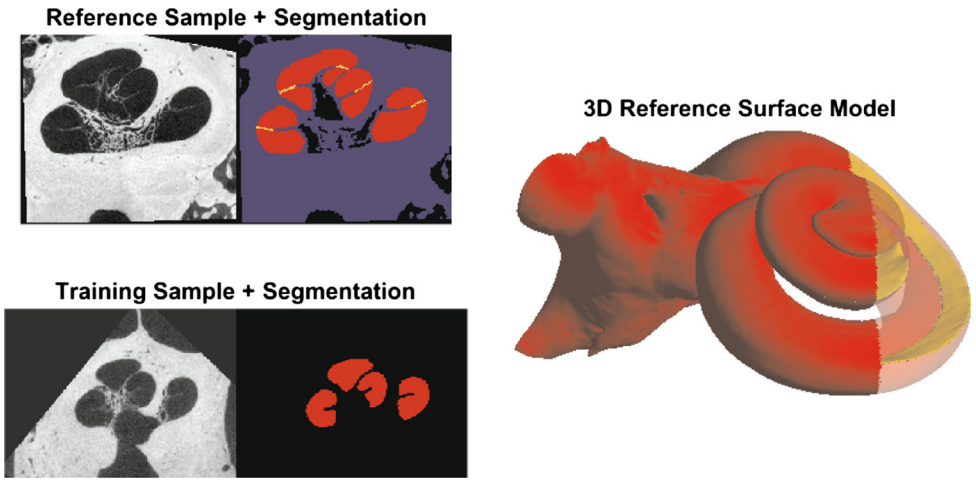

Fig. 1 Illustration of the training (left bottom) and reference data (left top) and the 3D reference surface model (right). The segmentation includes the scalae (red), background (black), bone (blue), and cochlear partition (yellow). The latter two were only segmented for the reference dataset

to obtain consistent quality and to ensure a smooth closing of the openings at the oval and round window.

Test data For the purpose of validating the SDM-fitting procedure, a test dataset is required. It consists of 14 samples (originating from eight different cadaverous head specimens), which were preserved with the Thiel preservation method [23]. The samples were scanned both with CBCT (ProMax® 3D Max, Planmeca, Finland) and μCT (μCT 100, Scanco Medical AG, Brüttisellen, Switzerland), and reconstructed in, respectively, 150 and 24.5 µm isotropic voxels.

Image processing and registration

The first part of the model building process involves creating correspondences via image registration between the reference and training data in order to describe the statistical variability. The full methodology is detailed in [11]. In short, the N training datasets, I_{M}, are in turn registered with the reference data, I_{F}, in two steps: rigid initialization followed by deformable registration.

A description of the non-rigid image registration stage is recapped here, with the relevant settings used for the data in this study. The registration task is cast as an optimization problem,

$$\hat{\mu} = \arg\min_{\mu} \mathcal{C}(T_{\mu}, I_{\mathrm{F}}, I_{\mathrm{M}}) \tag{1}$$

where a cost function $\mathcal{C}$ is minimized with respect to a transformation T_{μ}. Describing the volumetric data by their respective spatial domains, $\Omega_{\mathrm{F}} \subset \mathbb{R}^3$ and $\Omega_{\mathrm{M}} \subset \mathbb{R}^3$, this transformation maps points in the fixed domain to the moving, i.e., $T_{\mu} : \Omega_{\mathrm{F}} \rightarrow \Omega_{\mathrm{M}}$, and it is parametrized by the vector μ.

The `elastix` software library [13] is used for the implementation and optimization of the problem. A three-level cubic B-spline grid is chosen for the non-rigid transformation model. For the three levels, we use an isotropic grid point spacing of {60,18,6} voxels and an isotropic Gaussian smoothing with a kernel size of {6,2,1} voxels, respectively, thus starting with a coarse alignment which is gradually refined. Typically, the registration would be between the grayscale or segmented volumes. From experience, we know that it is then difficult to tune the various parameters involved to achieve good and consistent results because of the complexity and variation in the cochlear spiral shape. We found it beneficial to do a preprocessing step of the segmentations explicitly modeling the cochlear spiral, leading to an increased registration accuracy in the order of 20% for certain measures (see [11]). The strategy is to solve a partial differential equation for the cochlear volume representing the heat propagation through the cochlea starting from the apex as the hottest point. These heat maps encode a global similarity between the samples regardless of local differences, which can be used in the registration. The procedure is modified to favor an alignment of regions with similar heat, thereby capturing the cochlear spiral turning more realistically. This is expressed in the chosen cost function,

$$\mathcal{C} = \alpha \cdot \mathcal{S}_{\mathrm{Sim}}(\mu, H_{\mathrm{F}}, H_{\mathrm{M}}) + (1 - \alpha) \cdot \mathcal{P}_{\mathrm{BE}}(\mu) \tag{2}$$

where $\alpha = 0.9$ is an experimentally chosen weight parameter. The similarity, $\mathcal{S}_{\mathrm{Sim}}$, between the heat maps, H_{F} and H_{M}, is measured using sum of squared differences. The term $\mathcal{P}_{\mathrm{BE}}$ is the energy-bending regularization used to penalize strong changes and foldings in the transformation. The optimization is solved using adaptive stochastic gradient Descent [12] with a maximum of 1500 iterations. Only a subset (2^{18} random coordinates) of the voxel domain close to the cochlea was sampled for each iteration, in order to reduce the computational burden and focus the optimization to the area of interest. This was achieved by applying a binary sampling mask to the reference dataset, which was generated by dilating the cochlear segmentation with a spherical kernel

(radius = 20 voxels). These settings were fixed for all three levels of the registration.

Statistical deformation model construction

The output of the registrations ("Image processing and registration" section) is N=18 corresponding B-spline deformation fields, each one describing how the cochlear reference can deform to fit an instance of the training data. This information is built into a statistical deformation model (SDM) by applying a principal component analysis (PCA) over the B-spline parameters as described in [22]. It is a statistical description of the covariance of the deformation fields in a low dimensional space. The first mode of this space would typically describe the deformations changing the overall size of the cochlea. In order of decreasing influence, the remaining modes explain other shape changes, such as the cochlear turning. As it is a linear and generative model, it can be used to create deformation fields that deform the reference model according to the variation seen in the population (the training data), while ensuring that the output is still a valid cochlea. Building the SDM was done using the Statismo [15] software package. For additional details on SDMs we refer to [9,22]. The main advantage is that the model can be incorporated into a registration procedure where the reference μCT is fitted to a previously unseen conventional CT dataset (the target CT), as described in the following section.

SDM-regularized registration

1. Initialization The first step of the fitting procedure is to rigidly align the target CT scan to the position and orientation of the reference volume. In practice, it is difficult to know anything about the initial location of the cochlea in the CT images. An automatic initialization procedure could be developed, drawing inspiration from [17] or [21], but for this study the initialization was done using a landmark-based rigid transformation. The following four landmarks were placed manually in each dataset; the center of the round window at the bony overhang, the center of the modiolus, respectively, in the basal and apical turn, and finally the basal turn inner wall across from the round window [29]. The landmark transform is followed by a rigid image registration between the reference dataset and the CT scan. This step can provide a slight correction of the orientation and position in order to prevent a bias or uncertainty from the user-based landmarking.

2. Non-rigid registration Once the target CT and reference μCT are rigidly aligned, the deformable fitting process can be started, which is formulated as an image registration (see Eq. 1). The major modification is that the transformation model changes to a SDM-regularized cubic B-spline. In principle, this is a B-spline transform with the same grid definition as in the previously described registration model. However, each grid point cannot vary freely anymore. Instead, they deform in accordance with the learned covariance structure, which is described with a maximum of N modes of variation of the PCA. An implementation of this transformation type is available in the Statismo-`elastix` integration. The cost function can now be stated as,

$$\mathcal{C}_{\mathrm{SDM}} = \mathcal{S}_{\mathrm{Sim}}(\mu_{\mathrm{SDM}}, I_{\mathrm{F}}, I_{CT}), \tag{3}$$

where I_{F} is the reference μCT, and I_{CT} is a volume in CT resolution (e.g., one of the test datasets). As the reference data displays smaller structures not visible on the CT data, it can be considered a multimodality registration problem and we therefore use mutual information as the similarity metric. Further, a low degree of Gaussian smoothing was applied to the reference image (isotropic kernel size: 1.5 voxels). The blurring seems to have a negligible negative impact, as the difference in image resolution to the CT data is substantial. The optimization was done using adaptive stochastic gradient descent [12] with default settings, and 2^{15} random samples per iteration for a maximum of 500 iterations.

Evaluation

Cross-validation on training data All the training data contain a ground truth segmentation and are rigidly aligned with the reference data set, eliminating the need for the initialization step described in "SDM-regularized registration" section. The training data is first downsampled using a cubic interpolation kernel to 0.2 mm isotropic voxels in order to represent clinical training "CT" data. The SDM is built from the registrations of all the training samples except one. The SDM-fitting procedure is performed against the remaining sample with all available modes of variations. This is repeated for all training samples corresponding to a leave-one-out cross-validation of the SDM-fitting performance.

Generic measures The accuracy and precision are quantified with the Dice score of the binary segmentations, and with the bidirectional mean and maximum surface errors of the mesh models, as detailed in the following.

Let $L_{\mathrm{F}}(\mu_{\mathrm{SDM}})$ be the cochlear lumen segmentation after it has been fitted to a training CT image. We measure the overlap against the ground truth segmentation, L_{GT}, of the corresponding micro-CT image using the Dice score [6]:

$$\mathrm{DSC} = \frac{2 \cdot \left| L_{\mathrm{GT}} \bigcap L_{\mathrm{F}}(\mu_{\mathrm{SDM}}) \right|}{|L_{\mathrm{GT}}| + |L_{\mathrm{F}}(\mu_{\mathrm{SDM}})|} \tag{4}$$

Similarly, let $\mathbb{S}_{\mathrm{F}}(\mu_{\mathrm{SDM}})$ be the fitted 3D model, and $\mathbb{S}_{\mathrm{GT}}$ the ground truth surface extracted from each training micro-CT segmentation. There is no direct point correspondence between the surfaces, and they each contain a varying number

of vertices. The evaluation scores are therefore based on the closest points, i.e., the minimum Euclidean distance from a point, p, to any of the points, q, in the other surface, $\mathbb{S}$:

$$d(p, \mathbb{S}) = \min_{\forall q \in \mathbb{S}} \left(||p - q||_2 \right) \tag{5}$$

The mean surface error, $d_{\bar{s}}$, of each sample is then defined as the average of all the closest point distances:

$$d_{\bar{s}} = \frac{1}{N_{\mathrm{F}} + N_{\mathrm{GT}}} \left(\sum_{\forall p \in \mathbb{S}_{\mathrm{F}}(\mu_{\mathrm{SDM}})} d(p, \mathbb{S}_{\mathrm{GT}}) + \sum_{\forall p \in \mathbb{S}_{\mathrm{GT}}} d(p, \mathbb{S}_{\mathrm{F}}(\mu_{\mathrm{SDM}})) \right) \tag{6}$$

where N_{F} and N_{GT} are the total number of points in the respective surfaces.

The maximum surface error, d_m, is then similarly defined as the maximum of all the closest point distances:

$$d_{\mathrm{m}} = \max \left\{ \max_{\forall p \in \mathbb{S}_F(\mu_{\mathrm{SDM}})} d(p, \mathbb{S}_{\mathrm{GT}}), \max_{\forall p \in \mathbb{S}_{\mathrm{GT}}} d(p, \mathbb{S}_F(\mu_{\mathrm{SDM}})) \right\} \tag{7}$$

Landmark and morphology measures The above-mentioned generic measures are commonly reported and represent the overall performance in a general way. We supplement the evaluation with scores that highlight the errors at some specific landmark locations and with morphological differences, both serving to further illustrate the accuracy of the predicted shape. We manually placed the landmark of the cochlear apex, center of the round and oval window and measured the cochlear length, width and height according to the consensus definition of [26]. We further manually traced the ridge of the lamina spiralis from the scalae segmentation allowing us to provide a measure of the spiral length. The landmark placements and morphological measurements were done a single time by one rater for each training micro-CT dataset, the reference and for each predicted shape (i.e., the SDM-fit).

Test data As these datasets have no ground truth segmentations, our evaluation was restricted to include only the above-mentioned landmark and morphological (except spiral length) errors. The landmark placement and measurements of cochlear dimensions were made in the μCT test data, but the SDM is fitted to the CT data with 12 available modes of variations. The first 12 modes explain approximately 95% of the total variance in the training data. It is common practice to drop the remaining modes [9], as these are likely to represent noise in the training data and the model construction process. Note that μCT data were also carefully co-registered to its respective CT dataset, with a procedure using landmark initialization plus a rigid image registration, similar to the procedure described in "SDM-regularized registration" section.

Results and discussion

A qualitative evaluation of the SDM-fitting is illustrated in Fig. 2, and the statistics for the average predicted cochlear shape accuracy and precision are given in Table 1. The visualized test data were chosen to reflect this average performance, and not the best case scenario. The interpretation of the generic evaluation measures remains to be somewhat qualitative in nature, as the absolute values are difficult to evaluate on their own. The Dice score is in the high end and the mean surface error below the CT data voxel size, which is satisfactory.

Compared to the results in [17] our generic measures show an improvement (a Dice score of 0.88 vs. 0.75, a mean surface error of 0.11 vs. 0.20 mm and a max surface error of 0.58 vs. 0.80 mm, respectively). As we use different data sets, amount of training data and SSM methodology, it is difficult to pinpoint what is contributing to the improved results. In the following, we will argue for the benefits of our approach and for the novelty of our work.

We use more training data in comparison to [17], which should improve the anatomical variability captured in the statistical model. Nonetheless, more μCT training data would still be desirable. Perhaps more importantly, our data have a better resolution, which allows us to improve on the anatomical representation of the cochlea. We are able to model the cochlea as a single structure including the lamina spiralis, and then add the cochlear partition separately. This configuration gives a better potential for using the predicted cochlear shape in computational simulations, e.g., simulating [4,16,25] and analyzing [20,24] surgical CI-insertions.

A general advantage of the SDM procedure over the Active Shape Model approach [5,17] is that it can handle intra-anatomical structures nicely. Since the intracochlear anatomy is not visible in clinical CT images, there is no gradient information for guiding the fit. Further, as the training μCT data support is limited, it is currently not feasible to make credible statistical shape models of intracochlear structures on their own. With the SDM strategy everything is described as deformation fields, which lets the intracochlear structures passively follow the deformations based on the contrasted CT image information.

Besides the generic scores presented in Table 1, we have tried to bring forth additional measures for evaluating shape prediction accuracy in the form of anatomically specific scores. The apex error is shown to be larger than the maximum surface error, which demonstrates that the SDM and fitting

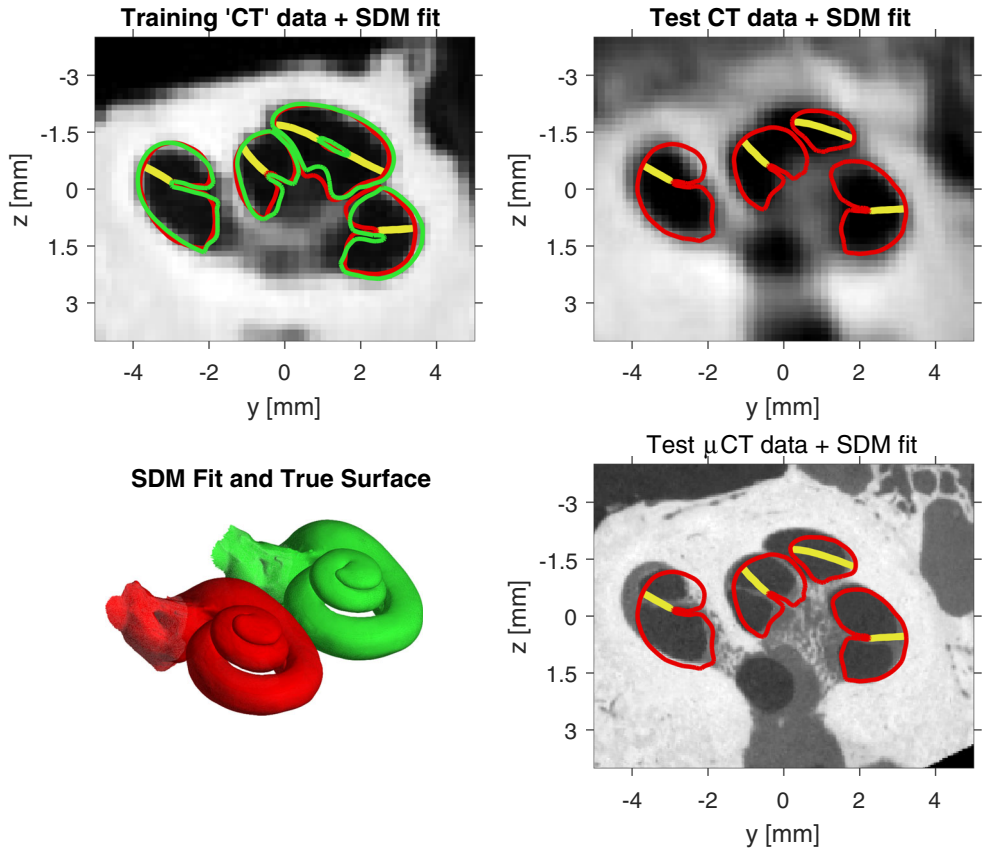

Fig. 2 Qualitative accuracy of the SDM-fit (red for cochlear scalae and yellow for cochlear partition) and comparison to the ground truth cochlear scalae segmentation (green) when available. The top left figure shows the fit on a training "CT" image, i.e., a downsampled μCT from the set of training data. The bottom left shows the corresponding 3D models shifted apart in order to get a global view of the correct and predicted cochlear shape. The top right figure shows the SDM-fit on a CT image from the set of test data, and finally the bottom right shows the same fit overlaid on the corresponding co-registered test μCT data

Table 1 Statistics of fitting performance, reported as the mean $\pm$ 1 standard deviation. Landmark scores are reported in number of voxels of the CT data

	Error measure	Cross-validation	Test data
Generic	Dice score	0.88 ± 0.02	–
	Mean surface error (mm)	0.11 ± 0.01	–
	Max surface error (mm)	0.58 ± 0.11	–
Landmark	Apex error (voxels)	4.2 ± 2.4	5.8 ± 3.0
	Oval window error (voxels)	1.3 ± 0.5	2.5 ± 1.6
	Round window error (voxels)	1.4 ± 0.8	1.8 ± 0.8
Morphologic	Cochlear length error (mm)	0.02 ± 0.2	-0.06 ± 0.4
	Cochlear width error (mm)	0.08 ± 0.2	-0.04 ± 0.2
	Cochlear height error (mm)	0.05 ± 0.2	0.05 ± 0.2
	Spiral length error (mm)	0.06 ± 1.1	–

procedure still have some limitations with the apical region of the cochlea. From the test data shown in Fig. 2, it can also be observed that the predicted cochlear outer edge can have slight offsets from the correct position. These limitations can be explained by a combination of two factors. First, the low resolution of the CT data results in relatively weak image gradients for guiding the fit. Second, the limited size of training data affects the precision of the model, since the learned modes of variation may not be able to sufficiently represent true regional independence. However, μCT data is a scarce source to work with and the required processing and segmentation are time consuming tasks. The limitations of

the model should be seen in this light, and its application can still be valuable. Providing a fair prediction of the cochlear anatomy can be more useful than assuming nothing about the anatomy, which is still the general practice today [18]. The remaining landmark and morphological measures show that the SDM procedure otherwise provides an accurate prediction, although the precision could be improved. The observed high standard deviation is also influenced by the uncertainty from the manual measurements and landmark placements. The exact errors should therefore be interpreted with some care, but they do provide a sense of the order of magnitude of the prediction accuracy.

In a real clinical scenario, the CT data might have additional noise and artefacts from patient motion, metal implants, etc. Since the fitting procedure is heavily constrained by the learned model, the method is expected to be robust against these disturbances, unless the images are severely corrupted. For certain applications and medical problems, a better performance might be required before the method can be used. On the other hand, the work of Noble et al. [18] has already demonstrated that these types of methods can be used in real life to modify CI programming. Since our method is more accurate at predicting the cochlea shape, we reason that our method can address the same problem with a performance that is at least on par.

The cochlear partition does not seem to fit very accurately on the test data (Fig. 2 bottom right). It is important to note two things in this regard. First, the basilar membrane is not visible in the CT data, meaning there is no image information to guide the fitting method to give a good result. Secondly, the variability of this structure is not modeled in the SDM. It is simply a passive structure following the fitting of cochlea. This is a reflection of how the partition was seen in the reference data, but we have no guarantee of how precise and representative that generally is.

The true test of usability would of course be a measure of improvement in hearing restoration outcomes in CI-users (following a procedure similar to [18]). However, such a measure would be influenced by many other confounding factors than just the accuracy of cochlear shape prediction, which is the scope of this study. Generally, we assume that a better shape prediction would positively correlate with improvements in CI hearing restoration.

Conclusion

Methods for predicting the cochlear shape from CT images allow for improvements in procedures regarding the CI surgery and postoperative CI audio processor programming. Using statistical shape models is a promising strategy, as it can allow for estimation of intracochlear anatomical features as well. We have here presented and evaluated an alternative method to the classical active shape model approach, and shown that it achieves an accuracy competitive with the current state of the art.

Acknowledgements The research leading to HEAR-EU results has received funding from the European Union Seventh Frame Programme (FP7/2007-2013) under Grant Agreement No. 304857.

Compliance with ethical standards

Conflict of interest The authors declare that they have no conflict of interest.

Human and animal rights This article does not contain any studies with human participants or animals performed by any of the authors. This articles does not contain patient data.

References

1. Avci E, Nauwelaers T, Lenarz T, Hamacher V, Kral A (2014) Variations in microanatomy of the human cochlea. J Comp Neurol. https://doi.org/10.1002/cne.23594
2. Baker G, Barnes N (2005) Model-image registration of parametric shape models: fitting a shell to the cochlea. Insight J
3. Braun K, Boehnke F, Stark T (2012) Three-dimensional representation of the human cochlea using micro-computed tomography data: presenting an anatomical model for further numerical calculations. Acta Oto Laryngol 132(6):603–613. https://doi.org/10.3109/00016489.2011.653670
4. Ceresa M, Mangado N, Andrews RJ, González Ballester MÁ (2015) Computational models for predicting outcomes of neuroprosthesis implantation: the case of cochlear implants. Mol Neurobiol 52(2):934–941
5. Cootes TF, Taylor CJ, Cooper DH, Graham J (1995) Active shape models—their training and application. Comput Vis Image Underst 61(1):38–59
6. Dice LR (1945) Measures of the amount of ecologic association between species. Ecology 26(3):pp. 297–302, http://www.jstor.org/stable/1932409
7. Erixon E, Rask-Andersen H (2013) How to predict cochlear length before cochlear implantation surgery. Acta Oto Laryngol 133(12):1258–1265. https://doi.org/10.3109/00016489.2013.831475
8. Escudé B, James C, Deguine O, Cochard N, Eter E, Fraysse B (2006) The size of the cochlea and predictions of insertion depth angles for cochlear implant electrodes. Audiol Neurotol 11(Suppl 1):2733. https://doi.org/10.1159/000095611
9. Heimann T, Meinzer HP (2009) Statistical shape models for 3D medical image segmentation: a review. Med Image Anal 13(4):543–563. https://doi.org/10.1016/j.media.2009.05.004
10. Ketten DR, Skinner MW, Wang G, Vannier MW, Gates GA, Neely JG (1998) In vivo measures of cochlear length and insertion depth of nucleus cochlear implant electrode arrays. Ann Oto Rhinol Laryn Supplement 175:116, http://europepmc.org/abstract/MED/9826942
11. Kjer HM, Vera S, Fagertun J, Gil D, González-Ballester MÁ, Paulsen R (2015) Image Registration of Cochlear μCT Data Using Heat Distribution Similarity. In: Image Analysis, Springer, pp 234–245, https://doi.org/10.1007/978-3-319-19665-7_20
12. Klein S, Pluim JPW, Staring M, Viergever MA (2009) Adaptive stochastic gradient descent optimisation for image registration. Int J

Comput Vis 81(3):227–239. https://doi.org/10.1007/s11263-008-0168-y
13. Klein S, Staring M, Murphy K, Viergever MA, Pluim JP (2010) Elastix: a toolbox for intensity-based medical image registration. IEEE Trans Med Imag 29(1):196–205
14. Lorensen WE, Cline HE (1987) Marching cubes: a high resolution 3D surface construction algorithm. SIGGRAPH Comput Graph 21(4):163–169. https://doi.org/10.1145/37402.37422
15. Lüthi M, Blanc R, Albrecht T, Gass T, Goksel O, Büchler P, Kistler M, Bousleiman H, Reyes M, Cattin P, Vetter T (2012) Statismo–a framework for PCA based statistical models. Insight J 1:1–18
16. Mangado N, Ceresa M, Duchateau N, Kjer HM, Vera S, Velardo HD, Mistrik P, Paulsen RR, Fagertun J, Noailly J, Piella G, González Ballester MÁ (2015) Automatic model generation framework for computational simulation of cochlear implantation. Ann Biomed Eng 44(8):2453–2463. https://doi.org/10.1007/s10439-015-1541-y
17. Noble JH, Labadie RF, Majdani O, Dawant BM (2011) Automatic segmentation of intracochlear anatomy in conventional CT. IEEE Trans Biomed Eng 58(9):2625–2632. https://doi.org/10.1109/TBME.2011.2160262
18. Noble JH, Labadie RF, Gifford R, Dawant B (2013) Image-guidance Enables New Methods for Customizing Cochlear Implant Stimulation Strategies. IEEE Trans Neural Syst Rehabil Eng 21(5):820–829. https://doi.org/10.1109/TNSRE.2013.2253333
19. Paulsen R, Baerentzen J, Larsen R (2010) Markov random field surface reconstruction. IEEE Trans Vis Comput Gr 16(4):636–646. https://doi.org/10.1109/TVCG.2009.208
20. Rau TS, Hussong A, Leinung M, Lenarz T, Majdani O (2010) Automated insertion of preformed cochlear implant electrodes: evaluation of curling behaviour and insertion forces on an artificial cochlear model. Int J Compu Assisted Radiol Surg 5(2):173–181
21. Reda FA, Noble JH, Labadie RF, Dawant BM (2012) Automatic pre- to intra-operative CT registration for image-guided cochlear implant surgery. IEEE Trans Biomed Eng 59(11):3070–3077. https://doi.org/10.1109/TBME.2012.2214775
22. Rueckert D, Frangi AF, Schnabel JA (2003) Automatic construction of 3-D statistical deformation models of the brain using nonrigid registration. IEEE Trans Med Imag 22(8):1014–1025. https://doi.org/10.1109/TMI.2003.815865
23. Thiel W (1992) The preservation of the whole corpse with natural color. Ann Anat Anat Anzeiger Off Organ Anat Ges 174(3):185–195
24. Todd CA, Naghdy F, Svehla MJ (2007) Force application during cochlear implant insertion: an analysis for improvement of surgeon technique. IEEE Trans Biomed Eng 54(7):1247–1255. https://doi.org/10.1109/TBME.2007.891937
25. Vera S, Perez F, Balust C, Trueba R, Rubió J, Calvo R, Mazaira X, Danasingh A, Barazzetti L, Reyes M, Ceresa M, Fagertun J, Kjer HM, Paulsen R, González Ballester MÁ (2014) Patient specific simulation for planning of cochlear implantation surgery. In: Workshop on clinical image-based procedures, Springer, Berlin, pp 101–108
26. Verbist BM, Skinner MW, Cohen LT, Leake PA, James C, Boëx C, Holden TA, Finley CC, Roland PS, Roland JT, Haller M, Patrick JF, Jolly CN, Faltys MA, Briaire JJ, Frijns JH (2010) Consensus panel on a cochlear coordinate system applicable in histologic, physiologic, and radiologic studies of the human cochlea. Otol Neurotol 31(5):722–730
27. Wang G, Vannier MW, Skinner MW, Cavalcanti MGP, Harding GW (1998) Spiral CT image deblurring for cochlear implantation. IEEE Trans Med Imag 17(2):251–262. https://doi.org/10.1109/42.700737
28. Wilson BS, Dorman MF (2008) Cochlear implants: a remarkable past and a brilliant future. Hearing Res 242(1–2):3–21. https://doi.org/10.1016/j.heares.2008.06.005
29. Wimmer W, Venail F, Williamson T, Akkari M, Gerber N, Weber S, Caversaccio M, Uziel A, Bell B (2014) Semiautomatic cochleostomy target and insertion trajectory planning for minimally invasive cochlear implantation. Biomed Res Int. https://doi.org/10.1155/2014/596498
30. Yushkevich PA, Piven J, Hazlett HC, Smith RG, Ho S, Gee JC, Gerig G (2006) User-guided 3D active contour segmentation of anatomical structures: significantly improved efficiency and reliability. Neuroimage 31(3):1116–1128